IEEE Access
Multidisciplinary ⋮ Rapid Review ⋮ Open Access Journal

Received 1 November 2022, accepted 18 November 2022, date of publication 1 December 2022,
date of current version 7 December 2022.

Digital Object Identifier 10.1109/ACCESS.2022.3225834

RESEARCH ARTICLE

A Comparison Between Tone-Based and Code-Based Cell Search Schemes for Multipath Division Multiple Access

JIA-LE YIN[1], WEI-HAN HSIAO[2], (Member, IEEE), MING-CHUN LEE[1], (Member, IEEE), AND CHIA-CHI HUANG[1]

[1]Institute of Communications Engineering, National Yang Ming Chiao Tung University (NYCU), Hsinchu 30010, Taiwan
[2]Department of Electrical Engineering, Chang Gung University (CGU), Taoyuan 33302, Taiwan

Corresponding author: Wei-Han Hsiao (whsiao@cgu.edu.tw)

This work was supported by the National Science and Technology Council of Taiwan under Grant 111-2221-E-A49-070 and Grant 111-2218-E-A49-024.

ABSTRACT Cell search procedure is an essential and critical process in an early stage when the user equipment (UE) is powered on. It mainly comprises symbol and frame timing synchronization, frequency offset compensation, and base station (BS) identification. Among the current exiting 3G, 4G and 5G mobile networks, the UE completes the initial cell search based on different code sequences. In this paper, we investigate and compare two kinds of cell search methodology. Tone-based and code-based methods are explored for massive antenna systems. The detailed description and analysis are offered for two approaches. Simulation results indicate that the tone-based cell search not only possesses stable performance with respect to path numbers but also outperforms the code-based one in general channel realizations in terms of cell search error probability. The results suggest that the tone-based cell search could be used for 5G communication systems.

INDEX TERMS Initial cell search, tone-based cell search, 5G, cellular systems, massive antennas.

I. INTRODUCTION

During mobile communication setup, initial cell search is a necessary process for link establishment between a UE and a serving BS. With the help of control signals, the procedure deals with time and frequency synchronization and performs home BS selection for the UE. Time synchronization consists of symbol and frame timing synchronization [1] for both BS and UE to be properly time aligned. On the other hand, frequency synchronization is to estimate and compensate for the integer carrier frequency offset (ICFO) and the fractional carrier frequency offset (FCFO) [2]. The frequency impairment originates from the oscillator mismatch between the transmitter and the receiver, and the Doppler shift due to mobility of the UE. Therefore, the initial cell search plays an essential role for the successful connection between BS and UE. Of the original 1G to current 5G mobile networks, the initial cell search is done in either frequency or time domains.

The associate editor coordinating the review of this manuscript and approving it for publication was Stefan Schwarz.

A. 1G TO 5G CELL SEARCH METHODS

The Advanced Mobile Phone System (AMPS) [3] is the first generation (1G) mobile communication systems based on analog signals developed by Bell Labs in the 1980s. The frequency reuse factor is 7, and each cell is divided into 3 sectors. Therefore, the number of Physical Cell IDs (PCI) is 21.

In AMPS system, each sector is assigned a control channel. The initial cell search is based on finding the control channel with the highest power to determine the home BS sector, which can be divided into the following two steps. (1) The first step is frequency scanning. After the UE is powered on, it scans those 21 control channels. The UE next sorts them in the order of decreasing power and selects the strongest one as the home BS. (2) The second step is Forward Control Channel (FCC) detection. This is for time synchronization, including bit synchronization and frame synchronization. We call this search method *Frequency Based Cell Search*.

The Global System for Mobile Communications (GSM) [3], [4] is the second generation (2G) mobile communication

system, which was widely used in the 1990s. Since then, both data signals and control channels are digitized. The frequency reuse factor is 4 (with frequency hopping) and each cell is divided into 3 sectors. Therefore, the number of PCI is 12.

The initial cell search of the GSM system can be divided into four steps. (1) The first step is frequency scanning. The UE scans all the control channels and arranges them in decreasing order according to their signal strength. (2) The second step is Frequency Correction CHannel (FCCH) check. The UE tunes to the strongest carrier frequency, and then confirms whether it is the Broadcast CHannel (BCH) through decoding an FCCH burst. (3) The third step is Synchronization CHannel (SCH) detection. This is for time synchronization. (4) The fourth step is Broadcast Control CHannel (BCCH) detection to acquire the system information. After completing the frequency and time synchronization, the UE can accurately read the home BS ID and other system information from the BCCH. So far, the initial cell search has been completed. This initial cell search method also belongs to *Frequency Based Cell Search*, like the AMPS system.

Wideband Code Division Multiple Access (WCDMA) [5], [6] is a third generation (3G) mobile communication system. The WCDMA system was widely used in the 2000s. The frequency reuse factor is 1, and each cell is divided into 3 sectors. The number of PCI is 512.

The initial cell search of the WCDMA system can be divided into three steps below [7], [8]. (1) The first step is Primary Synchronization CHannel (P-SCH) detection. The UE correlates the received signal with a known and unique Primary Synchronization Code (PSC) to obtain the exact slot timing. Typically, this can be done through a PSC matched filter. (2) The second step is Secondary Synchronization CHannel (S-SCH) detection. This is for frame timing synchronization and Scrambling Code Group (SCG) detection. 3GPP uses a total of 512 Scrambling Codes (SCs), divided into 64 groups, for 512 cell sectors. Each group contains 8 scrambling codes. The information of the SCG is carried in the S-SCH. After this step, we can determine which group it belongs to. (3) The third step is Common Pilot CHannel (CPICH) detection. This step is to select 1 SC from the SCG determined in Step 2. CPICH carries a SC of length 38400 chips. Each BS sector is assigned a SC. Once the scrambling code is detected, the PCI is also known. So far, the initial cell search has been completed. We call this initial cell search method *Code Based Cell Search*.

Long Term Evolution Advanced (LTE-A) [9], [10], [11] is the fourth generation (4G) mobile communication system, which was widely used in 2010s. The frequency reuse factor is 1 (with partial frequency reuse), and each cell is divided into 3 sectors. The number of PCI is 504.

The initial cell search of the LTE-A system is executed with the following three steps [12], [13], [14]. (1) The first step is initial synchronization. It is performed in the time domain. From the fact that the cyclic prefix (CP) is a copy of the tail part of OFDM symbols, we can estimate the symbol timing and fractional carrier frequency offset. (2) The second step is Primary Synchronization Signal (PSS) detection. This is performed in the frequency domain for slot timing synchronization, integer carrier frequency offset detection, and sector ID detection. The PCI index is determined from $N_{ID}^{cell} = 3N_{ID}^{(1)} + N_{ID}^{(2)}$, where $N_{ID}^{(1)}$ and $N_{ID}^{(2)}$ are Cell-Identity Group (CIG) and sector ID, respectively. The PCIs are divided into 168 groups. Note that $N_{ID}^{(1)} \in \{0 \sim 167\}$ and $N_{ID}^{(2)} \in \{0,1,2\}$. $N_{ID}^{(1)}$ is carried in the Secondary Synchronization Signal (SSS) and $N_{ID}^{(2)}$ is transmitted in PSS. Thus, 504 ($= 168 \times 3$) PCIs are assumed in LTE-A. (3) The third step is SSS detection. This step is for frame timing synchronization and Cell-Identity Group detection. After the above three steps, we have completed the process of initial cell search. Each BS sector of the LTE-A system corresponds to a set of codes (PSS+SSS). Since the initial cell search is based on detecting these two codes to find a home BS, this method belongs to *Code Based Cell Search*.

5G New Radio (5G-NR) is a fifth generation (5G) mobile communication system, which been commercially used since 2020s [15], [16], [17]. The frequency reuse factor is 1, and each cell is divided into 3 sectors. The PCI index is determined from $N_{ID}^{cell} = 3N_{ID}^{(1)} + N_{ID}^{(2)}$, where $N_{ID}^{(1)} \in \{0 \sim 335\}$ and $N_{ID}^{(2)} \in \{0,1,2\}$ are Cell-Identity Group and sector ID, respectively. Thus, 1008 ($= 336 \times 3$) PCIs are assumed in 5G-NR. Likewise, 5G-NR uses the similar cell search method as in the LTE-A, which is also a kind of *Code Based Cell Search*. A PSS based timing synchronization algorithm with anti-frequency offset and anti-noise is developed in [18]. It proposed improved coarse and fine timing synchronization algorithms based on Fourier theory and a triple autocorrelation algorithm. In [19], it presented a deep-learning based initial access method on mmWave bands. It used probability function for detection statistics, which is different from conventional ones that exploit energy detection. Reference [20] offered a physical-layer cell ID detection algorithm that employs a joint estimation for both the frequency offset and the SSS sequence. It adopted 5G-NR beamforming technique for the initial access at BSs. In [21], it proposed a network resolved and mobile assisted cell search, which lets the BSs be the main performers for deciding the appropriate home BS and UEs only be the role of assistants in the cell search process. As compared to the conventional cell search that requires the UE to detect the cell ID and decode the control data, a significant computation can be offloaded to the BSs that relieves the computational efforts and enhances power efficiency for the UE.

B. MOTIVATION AND CONTRIBUTIONS

To sum up, 1G and 2G use *Frequency Based Cell Search*, 3G, 4G, and 5G use *Code Based Cell Search* [22]. In this article, we compared tone-based cell search method with code-based method. We will introduce and analyze both cell search methods in detail, and the performance is evaluated on a 5G multipath division multiple access (MDMA) system.

Contributions of this paper are described as follows.

1. Current and previous use of initial cell search methods are listed and compared, which shows that the 3G,

TABLE 1. Notations used throughout the article.

Notation	Meaning
M	Number of BS antennas
J	Number of users in each cell
L	Number of resolvable paths
N	FFT size
N_{CP}	Cyclic prefix duration
θ	Symbol time offset
ε	Carrier frequency offset
ε_I	Integer carrier frequency offset
Δ	Control tone spacing between two nearest SCTs
β	Path loss
ζ	Shadow fading
$s_j^{\rho,m}[n]$	Transmit signal at the m-th antenna from BS ρ to user j
$h_j^{\rho,m}[l]$	The l-th path of the channel impulse response at the m-th antenna between BS ρ to user j
D	Control data
$x_j^{\rho}[n]$	User data from BS ρ to user j
$\Theta_j^{\rho,m}[n]$	Data of the user j after pre-RAKE precoding at antenna m of BS ρ
$w[n]$	Additive white Gaussian noise
$z[n]$	Received signal without timing offset and carrier frequency offset
$r_j[n]$	Received signal of the user j
$R_j[k]$	FFT output of $r_j[n]$
$\mathbf{c}_\rho[n]$	Code sequence of BS ρ
$*$	Convolution operator
$\delta[\cdot]$	Kronecker delta function
gcd(a,b)	The greatest common divisor of a and b

4G and 5G mobile networks all rely on code-based cell search.

2. The detailed description and analysis are offered for both code and tone-based cell search.

3. Simulation results indicate that the tone-based cell search outperforms the code-based one in general channel realizations in terms of cell search error probability.

4. It is found that the tone-based cell search possesses stable performance which is nearly invariant to path numbers.

The paper is organized as follows. Sec. II shows the MDMA system architecture, including the channel model and frame structure. Sec. III gives the detail of the tone-based cell search. Sec. IV then provides the code-based cell search. Sec. V shows simulation results to evaluate cell search performance in terms of cell search error probability. Finally, the paper concludes in Sec. VI.

The notations and the meanings thereof in the whole paragraphs are described in Table 1. The bold face in lower and upper cases are used respectively for vectors and matrices.

II. MDMA SYSTEM OVERVIEW

MDMA is one of the multiple access techniques for 5G mmWave communication systems [23]. It greatly simplifies

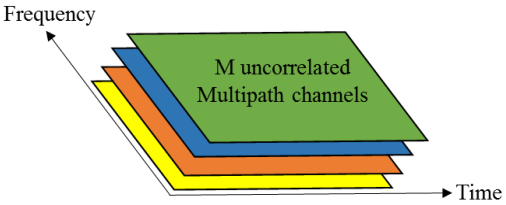

FIGURE 1. *M* **uncorrelated multipath channels.**

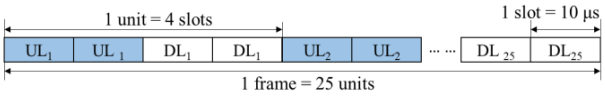

FIGURE 2. Frame structure of MDMA.

computation burden at UE terminals whereas it endows the BS with powerful processing capabilities. The BS acquires multipath diversity by Pre-RAKE precoding and RAKE equalizer at transmitters and receivers, respectively. Moreover, MDMA obtains large processing gain to suppress interference by deploying massive antennas at BSs, which is feasible for mmWave communications. Antennas at BSs are separately placed tens of wavelengths apart to be of low correlation. Thus, MDMA exploits both time and spatial degrees of freedom to separate users from each other. Each user owns equivalently M uncorrelated multipath channels at both time and frequency domains as shown in Fig. 1, where M is the number of BS antennas. The details are revealed in [24] and [25] for readers of interest. In brief, the benefits of using MDMA are channel hardening, uniform data rate, high cellular capacity, spatial focus beamforming, and hybrid multiple access.

Fig. 2 is the frame structure for MDMA at mmWave band of 30 GHz. The smallest transmission unit contains four time slots, with two uplink (UL) slots followed by two downlink (DL) slots. 25 units composes of one frame of 1 ms. Since the coherence time, which is $(5f_{\mathrm{d}})^{-1}$, at 30 GHz band is roughly 20 μs for a vehicular speed of 300 km/hr, the consecutive two time slots of 20 μs experience nearly the same channel response. Thus, the channel estimate at the first UL slot can be used not only for BS equalizer but also for the Pre-Rake precoding in the first DL slot. The second UL slot is used in the same manner for the second DL slot. Note that the channel estimate in MDMA is completed with the aid of different pilots sent from each user in the uplink [26].

The channel bandwidth considered is 200 MHz allocated for each user at the same piece of spectrum. OFDM modulation is used for the purpose of cell search. FFT size and subcarrier spacing are 2048 and 100kHz, respectively. The sampling time is about 5ns. On the other hand, single carrier modulation, say BPSK, is employed for data transmission. The processing gain derived from massive BS antennas is used to suppress both intra-cell and inter-cell interferences. Besides, the MDMA is interference limited with power control [25]. In addition, control channels are designed in both time and frequency domains. For the following discussion, tone-based and code-based cell search methods are

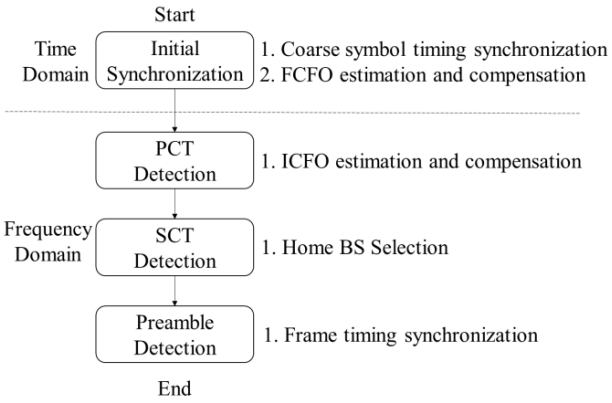

FIGURE 3. Procedure for the tone-base cell search.

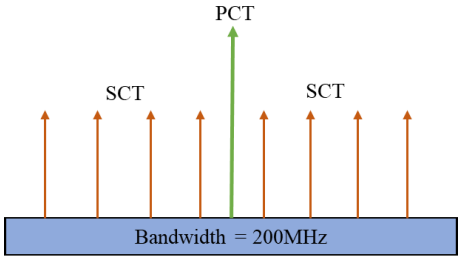

FIGURE 4. Subcarriers for control signaling.

corresponding to frequency-domain and time-domain control channel designs, respectively.

III. TONE-BASED CELL SEARCH

The procedure for the tone-base cell search is presented in Fig. 3. It is composed of four essential steps. In the first step, the initial synchronization detects symbol timing and also estimates and compensates for FCFO. The following primary control tone (PCT) detection estimates ICFO and compensates for it accordingly. Next, secondary control tone (SCT) detection identifies the cell ID. Finally, preamble detection finds the exact frame timing.

The subcarriers for control signaling shown in Fig. 4 are developed for tone-based cell search, which consists of one PCT and eight SCTs. PCT is at the central subcarrier while 8 SCTs are separated at equal distance with one another. The first SCT starts with a position index ρ, which is its cell ID. Consider a typical cellular system with a home cell and four tiers of cochannel cells. Each cell is composed of three sectors. There are totally 61 $(= 1 + 6 + 12 + 18 + 24)$ cochannel cells. Hence, at least 183 $(= 61 \times 3)$ cell IDs are needed. In the MDMA system, the position of SCTs is designed to be distinct for each cell. It is achievable to distinguish all cells from each other since $183 \times 8 + 1 < 2048$, where 1 accounts for the PCT.

The SCTs are equally spaced over the entire transmission bandwidth, say 200 MHz with FFT size of 2048 for the system under consideration. Equal spacing assignment helps exploit the frequency diversity. Since there are eight SCTs for each sector, the frequency spacing for two adjacent SCTs is thus 200MHz/8 $=$ 25 MHz. The allocation of SCTs is

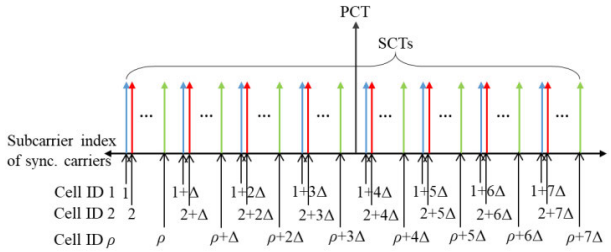

FIGURE 5. Illustration of control signaling subcarrier mapping of one OFDM symbol.

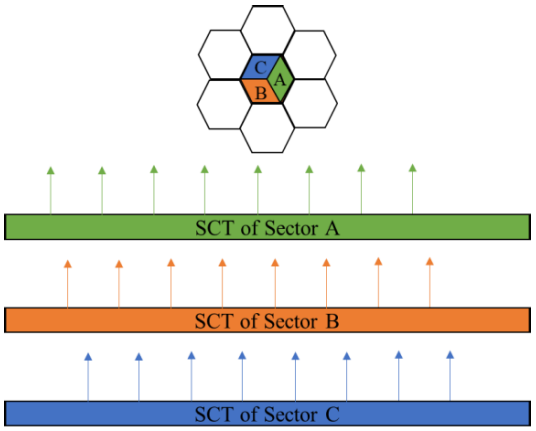

FIGURE 6. Example of SCTs for three sectors in the central cell.

TABLE 2. Mapping of the subcarrier index with respect to cell ID.

Cell ID	1	…	ρ	…	183
Subcarrier index	1, 1+Δ 1+2Δ, … 1+7Δ	…	ρ, ρ+Δ, ρ+2Δ, … ρ+7Δ	…	183, 183+Δ, 183+2Δ,… 183+7Δ

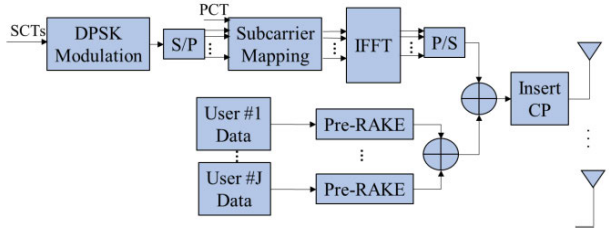

FIGURE 7. Downlink transmitter for tone-based cell search.

depicted in Fig. 5 below for 183 cell IDs. Δ denotes the control tone spacing between two nearest SCTs, i.e., $\Delta = 256$ due to 2048/8. The mapping result is also shown in Table 2 for clarity. An example of SCTs for three sectors in the central cell is plotted in Fig. 6.

The downlink transmitter for tone-based cell search is given in Fig. 7. The PCT is a single tone on the fixed subcarrier. On the other hand, the SCTs are modulated through DPSK on specific subcarriers. The mapping rule is corresponding to its own cell ID as mentioned before. An example can be referred to in [27]. The transmit power for the PCT is allocated half of a user power while the transmit power for the whole SCTs is equal to 1.5 times of a user power. After subcarrier mapping, the frequency domain control data is sent

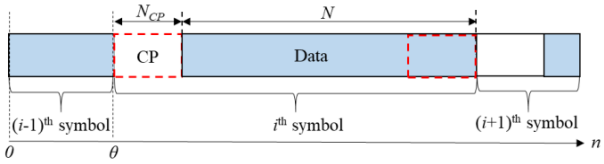

FIGURE 8. Received timing diagram.

to the conventional OFDM transmitter. In contrast, the user data is transmitted with single carrier modulation. Each active user data is first pre-equalized with Pre-RAKE precoding and then summed over all users. For the purpose of initial symbol timing synchronization, CP is inserted after the Pre-RAKE precoder. Finally, the time-domain control signals (w.r.t. PCT and SCT) and user data are transmitted by BS antennas.

To obtain antenna hopping diversity, one out of M' antennas are randomly selected for time-domain control data transmission on a slot by slot basis. On the selected antenna, the time-domain control data is sample-wise combined with user data for transmission. M antennas are preserved in advance, where $M' < M$ and M is the total number of BS antennas.

The transmit signal at the m-th antenna from BS ρ to user j, having SCT, can be generally written as

$$s_j^{\rho,m}[n] = \frac{1}{N}\sum_{k=0}^{N-1}\left(\underbrace{\sqrt{\frac{N}{2}}\delta[k-\frac{N}{2}]}_{\text{PCT}} + \underbrace{\sum_{p=1}^{8}\sqrt{\frac{3N}{16}}d_p^{\rho}\cdot\delta[\rho+k-\Delta\cdot p]}_{\text{SCT}}\right)e^{j\frac{2\pi kn}{N}} + \sum_{j=1}^{J}\underbrace{\sum_{l=0}^{L-1}\left(h_j^{\rho,m}[l]\right)^{*}\cdot x_j^{\rho}[n+l]}_{\triangleq\Theta_j^{\rho,m}} \tag{1}$$

where l, p, N, Δ, and $\delta[\cdot]$ denote path index, control data index, FFT size, and control tone spacing between two nearest SCTs, and Kronecker delta function, respectively. d and $x[\cdot]$ are control data (SCT) and user data. h is the channel impulse response at the m-th antenna between BS ρ to user j. $d \in\{\pm 1\}$ is due to DPSK modulation. For convenience, $\Theta_j^{\rho,m}$ is defined as data of the user j after pre-RAKE precoding at antenna m. The factor of $3N/16$ in the SCT results from the individual power of 8 SCTs having totally 1.5 times of a user power. The factor of $N/2$ in the PCT corresponds to half of a user power. The first and the second terms in (1), i.e., PCT and SCT, only appear at one of M' antennas as described in the last paragraph.

The detail steps for the tone-base cell search are introduced as follows.

A. INITIAL SYNCHRONIZATION

The received signal without timing offset (TO) and carrier frequency offset (CFO) is denoted as $z(n)$. The amount of TO and CFO are represented as θ and ε, respectively. The received signal with additive white Gaussian noise $w(n)$ is thus written as

$$r(n) = z(n-\theta)\exp(j2\pi\varepsilon n/N) + w(n), \tag{2}$$

where N is the FFT size. Since CP is the circular repetition from the last several samples of an OFDM symbol, we can estimate θ and ε by comparing the CP and the tail of the OFDM symbol, as shown in Fig. 8. To alleviate the noise effect, the minimum mean-square error (MMSE) criterion is used to estimate θ and ε as follows [21]:

$$\begin{aligned}(\hat{\theta},\hat{\varepsilon}) &= \arg\min_{\theta,\varepsilon}\left\{\sum_{n=\theta}^{\theta+N_{CP}-1}\left|r(n+N)e^{-j2\pi\varepsilon}-r(n)\right|^2\right\}\\ &= \arg\max_{\theta,\varepsilon}\left\{\begin{array}{l}2\mathrm{Re}\{\sum_{n=\theta}^{\theta+N_{CP}-1}r(n)r^*(n+N)e^{j2\pi\varepsilon}\}\\ -\sum_{n=\theta}^{\theta+N_{CP}-1}(|r(n)|^2+|r(n+N)|^2)\end{array}\right\}\\ &= \arg\max_{\theta,\varepsilon}\left\{\begin{array}{l}2\left|\sum_{n=\theta}^{\theta+N_{CP}-1}r(n)r^*(n+N)\right|\cos(\angle\gamma(\theta)+2\pi\varepsilon)\\ -\sum_{n=\theta}^{\theta+N_{CP}-1}(|r(n)|^2+|r(n+N)|^2)\end{array}\right\},\end{aligned} \tag{3}$$

where N_{CP} is the number of samples of the CP and $\gamma(\theta) = \sum_{n=\theta}^{\theta+N_{CP}-1} r(n)r^*(n+N)$. Thus,

$$\hat{\theta}_{MMSE} = \arg\max_{\theta}\left\{\begin{array}{l}2\left|\sum_{n=\theta}^{\theta+N_{CP}-1}r(n)r^*(n+N)\right|\\ -\sum_{n=\theta}^{\theta+N_{CP}-1}\left[|r(n)|^2+|r(n+N)|^2\right]\end{array}\right\}, \tag{4}$$

$$\hat{\varepsilon}_{MMSE} = -\frac{1}{2\pi}\angle\gamma(\hat{\theta}_{MMSE}), \tag{5}$$

where (4) and (5) are the estimated TO and FCFO, respectively. (4) is found by one-dimensional sequential line search. The symbol timing is thus obtained and the FCFO can be compensated afterwards [28]. The received timing is said to be correct, if the estimated symbol timing is located in the ISI free region.

B. PCT DETECTION

Based on (1), the received signal of the user j is expressed as in (6), shown at the bottom of the next page, where β^{ρ}, ζ^{ρ}, and $*$ represent path loss, shadow fading, and convolution operator, respectively. Converting into frequency domain via OFDM demodulation, we have, as in (7), shown at the bottom of the next page, where FFT$\{.\}$ is the FFT operation, $\gamma^{\rho} = (\beta^{\rho})^{1/2}\zeta^{\rho}e^{j2\pi k\theta/N}$, θ is the symbol time offset, and ε_I is the ICFO.

The detected PCT subcarrier is the one with the maximum subcarrier power. In order to obtain more accurate

PCT location index, we can accumulate over several slots. That is,

$$\hat{k}_j = \arg\max_k \left\{ \sum_i \left| R_{j,i}[k] \right|^2 \right\}, \tag{8}$$

where i denotes slot index. The ICFO is thus derived as

$$\hat{\varepsilon}_I = \frac{N}{2} - \hat{k}_j. \tag{9}$$

C. SCT DETECTION

Since the position of the SCTs is related to the cell ID, we can identify the cell ID by

$$\hat{k}_{\mathrm{ID}} = \arg\max_k \sum_i \sum_{p=1}^{8} \left| R_{j,i}[k + \Delta \cdot p] \right|^2. \tag{10}$$

Similar to (8), accumulating over more slots leads to better detection results.

D. PREAMBLE DETECTION

After the cell ID is identified from (10), the control data can be detected on the corresponding SCTs through DPSK demodulation. The preamble sequence used in MDMA is the 8-bit Hadamard Walsh code placed in the downlink slots of the first transmission unit in a frame. Thus, the frame timing synchronization is achieved by recognizing the preamble sequence.

Until now, the tone-based cell search has been completely introduced. For hardware design point of view, please refer to [27] for implementation purpose.

IV. CODE-BASED CELL SEARCH

The procedure for the code-base cell search is given in Fig.9. The main steps include initial synchronization, PCT detection, preamble detection, and cell ID detection. Different from the tone-based cell search, the preamble is detected before the cell ID is identified in the code-base cell search. The code adopted here is the popular Zadoff-Chu (ZC) sequence [29] used in current 4G systems. The generation of a ZC sequence, $\mathbf{c}_q$, follows the formula

$$\mathbf{c}_q[n] = \begin{cases} \exp\left\{ \dfrac{-j\pi}{N_{ZC}} q(n+1)n \right\}, & N_{ZC} \text{is odd} \\ \exp\left\{ \dfrac{-j\pi}{N_{ZC}} qn^2 \right\}, & N_{ZC} \text{is even} \end{cases}, \tag{11}$$

$$\begin{aligned} r_j[n] &= \sum_\rho (\beta^\rho)^{1/2} \cdot \varsigma^\rho \sum_m s_j^{\rho,m}[n] * h_j^{\rho,m}[n] + w_j[n] \\ &= \underbrace{\sum_\rho (\beta^\rho)^{1/2} \cdot \varsigma^\rho \cdot \frac{1}{N} \sum_{k=0}^{N-1} \left(\sqrt{\frac{N}{2}} \delta[k - \frac{N}{2}] \right) e^{j2\pi kn/N} * h_j^{\rho,m}[n]}_{\text{w.r.t. PCT}} \\ &\quad + \underbrace{\sum_\rho (\beta^\rho)^{1/2} \cdot \varsigma^\rho \cdot \tfrac{1}{N} \sum_{k=0}^{N-1} \left(\sum_{p=1}^{8} \sqrt{\tfrac{3N}{16}} d_p^\rho \cdot \delta[\rho + k - \Delta \cdot p] \right) \cdot e^{j2\pi kn/N} * h_j^{\rho,m}[n]}_{\text{w.r.t. SCT}} \\ &\quad + \underbrace{\sum_\rho \sum_m (\beta^\rho)^{1/2} \cdot \varsigma^\rho \cdot \sum_{j=1}^{J} \Theta_j^{\rho,m}[n] * h_j^{\rho,m}[n]}_{\text{w.r.t. user data}} + w_j[n], \end{aligned} \tag{6}$$

$$\begin{aligned} R_j[k] &= \mathrm{FFT}\left\{ r_j[n] \right\} \\ &= \underbrace{\sum_\rho \gamma^\rho \sqrt{\frac{N}{2}} \delta[k - \frac{N}{2} - \varepsilon_I] H_j^{\rho,1}[k - \varepsilon_I]}_{\text{w.r.t PCT}} \\ &\quad + \underbrace{\sum_\rho \sum_m \sum_{p=1}^{8} \gamma^\rho \sqrt{\frac{3N}{16}} d_p^\rho \delta[\rho + k - \Delta \cdot p - \varepsilon_I] H_j^{\rho,m}[k - \varepsilon_I]}_{\text{w.r.t. SCT}} \\ &\quad + \underbrace{\sum_\rho \sum_m \gamma^\rho \mathrm{FFT}\left\{ \sum_{j=1}^{J} \Theta_j^{\rho,m}[n] \right\} H_j^{\rho,m}[k - \varepsilon_I]}_{\text{w.r.t. User data}} \\ &\quad + W_j[k - \varepsilon_I], \end{aligned} \tag{7}$$

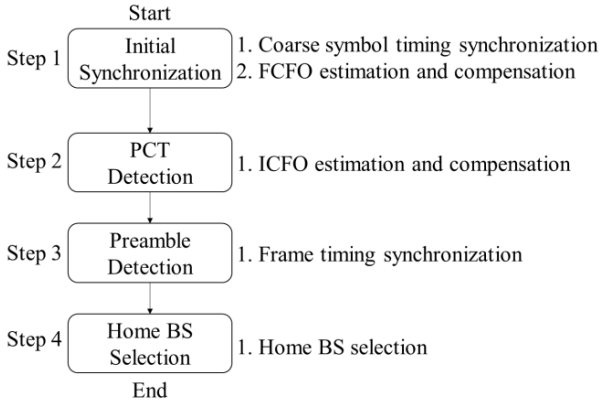

FIGURE 9. Procedure for the code-based cell search.

where q and N_{ZC} are root index and the length of the sequence, respectively. Besides, q and N_{ZC} are mutually prime, i.e., $\gcd(q, N_{ZC}) = 1$. In addition, distinct root indices yield different ZC sequences satisfying $\gcd(q_1, N_{ZC}) = \gcd(q_2, N_{ZC}) = 1$ and $\gcd(q_1 - q_2, N_{ZC}) = 1$ for $q_1 \neq q_2$. For multiple root indices, N_{ZC} must be a prime (and odd) number. Given two sequences $\mathbf{a}$ and $\mathbf{b}$ with equal length N, their auto-correlation function (ACF) and the cross-correlation function (CCF) at a phase shift τ are defined respectively as

$$R_{\mathbf{a}}[\tau] = \mathbf{a}^H \mathbf{a}^{(\tau)}, \tag{12}$$

$$R_{\mathbf{a},\mathbf{b}}[\tau] = \mathbf{a}^H \mathbf{b}^{(\tau)}, \tag{13}$$

where $\mathbf{a}^{(\tau)} = [a_{N-\tau}, a_{N-\tau+1}, \ldots a_{N-1}, a_0, a_1, \ldots a_{N-\tau-1}]^T$ and $\mathbf{a} = [a_0, a_1, \ldots\ a_{N-2}, a_{N-1}]^T$. For $q \neq \tilde{q}$, the two ZC sequences of length N_{ZC} have the following properties:

$$R_{\mathbf{c}_q}[\tau] = N_{ZC}\delta[\tau], \tag{14}$$

$$|R_{\mathbf{c}_q \cdot \mathbf{c}_{\tilde{q}}}[\tau]| = \sqrt{N_{ZC}}. \tag{15}$$

In many practical cases, the length of a ZC sequence may not be a prime number. We can first generate the ZC sequence having the prime length that is closest to and greater than the desired size. Next, truncate the ZC sequence from the last to the wanted size. For example, if the preferred length is 2048, one can first generate the ZC sequence of a prime length 2053 and then truncate the last five symbols to yield the desired length [30].

For the truncated sequence, denoted as $\widehat{c}_q$, the ACF and CCF turn to be

$$\left|R_{\widehat{c}_q}[\tau]\right| \leq N_{ZC}\delta[\tau] + (N_{ZC} - N + 2|\tau|), \tag{16}$$

$$|R_{\widehat{c}_q, \widehat{c}_{\tilde{q}}}[\tau]| \leq \sqrt{N_{ZC}} + (N_{ZC} - N + 2|\tau|), \tag{17}$$

where $\delta[.]$ is the Kronecker delta function. The proof is shown in the appendix.

The downlink transmitter for code-based cell search is given in Fig.10. Denote M as the total number of BS antennas. The PCT signal on the fixed subcarrier is a single tone, which broadcasts on every downlink slot. The control data is DPSK modulated and code spread by a ZC sequence. For antenna hopping diversity, one out of M' antennas are

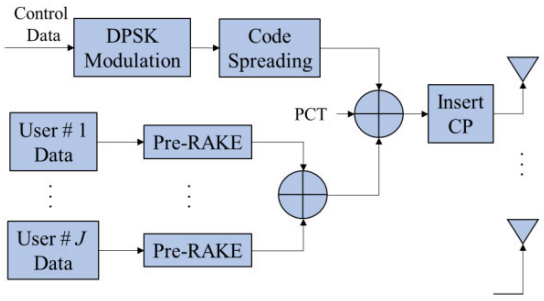

FIGURE 10. Downlink transmitter for code-based cell search.

randomly selected for control signals (PCT and control data), where M' is fixed and selected in advance. For user data, it is processed in the same way as described in Sec III. Note that CP is added for initial synchronization as in the tone-based cell search.

The transmit signal at the m-th antenna from BS ρ to user j can be generally written as

$$s_j^{\rho,m}[n] = \underbrace{\frac{1}{N}\sum_{k=0}^{N-1}\left(\sqrt{\frac{N}{2}}\delta[k - \frac{N}{2}]\right)e^{j2\pi kn/N}}_{\text{PCT}} + \underbrace{\sqrt{\frac{3}{2}}d_j^{\rho}\mathbf{c}_{\rho}[n]}_{\text{Control data}} + \sum_{j=1}^{J}\underbrace{\sum_{l=0}^{L-1}\left(h_j^{\rho,m}[l]\right)^* \cdot x_j^{\rho}[n+l]}_{\triangleq \Theta_j^{\rho,m}}, \tag{18}$$

where $\mathbf{c}_{\rho}[n]$ is the ZC sequence and N is the FFT size. $d_j^{\rho} \in \{\pm 1\}$ due to DPSK modulation. $\Theta_j^{\rho,m}$ is defined as data of the user j after pre-RAKE precoding at antenna m. The factor of 3/2 in (18) is equal to 1.5 times of a single user power for control data, which is the same as the total SCT power for fair comparison. The downlink slots in the first unit of each frame are related to the preamble for the code-based cell search.

Below we describe each step in the code-base cell search. The initial cell search and PCT detection follow the same approaches as in the tone-based search.

A. INITIAL SYNCHRONIZATION

Since the CP is inserted for the code-based cell search, the initial synchronization is the same as in the tone-based cell search to obtain symbol timing and FCFO. Please refer to the detail in Sec. III-A.

B. PCT DETECTION

Since the PCT is transmitted with identical parameters and settings for both tone- and code-based cell search, the same detection method, i.e., (6) to (9), is applied to complement for ICFO. Please refer to the detail in Sec. III-B.

C. PREAMBLE DETECTION

The length of ZC sequences is equal to the FFT size N. $N = 2048$ is used in simulations later. For the need of 183 cell

IDs, we can choose 8 root indices, say $q = 1, 2, \ldots 8$, and cyclically shift each sequence 23 times to obtain $8 \times 23 = 184$ sequences. The choice of the root indices and shift amount will be explained in Sec. V. The first sequence, denoted as $\mathbf{c}_0$, is selected to be the preamble sequence for all cells. The rest $\mathbf{c}_1, \mathbf{c}_2, \ldots, \mathbf{c}_{183}$ are used as code sequences for 183 cochannel cells.

The received signal in the first and the second downlink slot can thus be expressed as in (19), shown at the bottom of the next page.

Without loss of generality, assume user j is served by cell 1 and the first antenna is used for control signals. Then (19) can be further written as

$$\begin{aligned} r_j[n] &= \sqrt{\frac{3}{2}}(\beta^1)^{1/2} \cdot \varsigma^1 \cdot d^1 \mathbf{c}_0[n] * h_j^{1,1}[n] + \textit{interference} \\ &= \sqrt{\frac{3}{2}}\gamma^1 d_j^1 \sum_{l=0}^{L-1} h_j^{1,1}[l] c_0[(n-l) \bmod N] \\ &\quad + \textit{interference}, \end{aligned} \tag{20}$$

where $\gamma^1 = (\beta^1)^{1/2}\varsigma^1$. The *interference* combines PCT signal, other cell preamble signal, noise, and user data from all cells. The vector expression for N received time samples is

$$\begin{aligned} \mathbf{r}_j[n] &= \left[r_j[0] r_j[1] \cdots r_j[N-1]\right] \\ &= \sqrt{\frac{3}{2}}\gamma^1 d^1 \sum_{l=0}^{L-1} h_j^{1,1}[l] \cdot \mathbf{c}_0^{(l)} + \mathbf{I}, \end{aligned} \tag{21}$$

where $\mathbf{I}$ is the corresponding vectorization of the interference and $\mathbf{c}_0^{(l)}$ is the l-tap cyclic shift of the vector $\mathbf{c}_0$. Note that the exact mathematical expression is given as follows:

$$\mathbf{c}_0^{(l)} \triangleq \left[c_0[l] \cdots c_0[N-1]\ c_0[0] \cdots c_0[l-1]\right]. \tag{22}$$

As demonstrated in Fig. 11, the preamble sequence is used to match the received signal $r_j[n]$. This can be put in the matrix form as

$$\mathbf{R}_j = \mathbf{A}_0 \cdot \mathbf{r}_j = \left[R_j[0] R_j[1] \cdots R_j[L-1]\right], \tag{23}$$

where

$$\mathbf{A}_0 \triangleq \frac{1}{N}\begin{bmatrix} c_0^*[0] & c_0^*[1] & \cdots & c_0^*[N-1] \\ c_0^*[N-1] & c_0^*[0] & \cdots & c_0^*[N-2] \\ \vdots & \vdots & \ddots & \vdots \\ c_0^*[N-L+1] & c_0^*[N-L+2] & \cdots & c_0^*[N-L] \end{bmatrix}. \tag{24}$$

The path selection is then executed that selects N_p paths from $\mathbf{R}_j$. This thus gives:

$$\begin{aligned} \hat{\mathbf{R}}_j &= f(\mathbf{R}_j) = \left[R_j[\tau_1] R_j[\tau_2] \cdots R_j[\tau_{N_p}]\right], \\ \tau_k &\in \{0, 1, \ldots, L-1\}, \end{aligned} \tag{25}$$

where τ_k is the delay of selected path index, $f(\cdot)$ represents the path selection process as in [31].

The detected preamble is the one with the maximum power. The frame timing is identified accordingly. That is,

$$\hat{i} = \arg\max_i \left\{ \sum_{p=1}^{N_p} \left|R_{j,i}[\tau_p]\right|^2 \right\}, \tag{26}$$

where i denotes slot index for frame header.

D. CELL ID DETECTION

The cell ID is detected in the similar way as preamble detection. The receiver needs to identify which code sequence $\mathbf{c}_\rho$, $\rho = 1, 2, \ldots 183$, is transmitted for the received signal. Likewise, assume the first antenna is used for control signals. The received signal in the i-th downlink slot ($i \geq 3$) for user j served by cell ρ is vectorized as

$$\begin{aligned} \mathbf{r}_j^i &= \left[r_j^i[0] r_j^i[1] \cdots r_j^i[N-1]\right] \\ &= \sqrt{\frac{3}{2}}\gamma^\rho d_{j,i}^\rho \sum_{l=0}^{L-1} h_{j,i}^{\rho,1}[l] \cdot \mathbf{c}_\rho^{(l)} + \mathbf{I}, \end{aligned} \tag{27}$$

where $\gamma^\rho = (\beta^\rho)^{1/2}\varsigma^\rho$, $\mathbf{I}$ is the corresponding vectorization of the interference and $\mathbf{c}_\rho^{(l)}$ is the l-tap cyclic shift of the vector $\mathbf{c}_\rho$. Note that $r_j^i[n]$ is of the similar form as (20), i.e.,

$$r_j^i[n] = \sqrt{\frac{3}{2}}(\beta^\rho)^{1/2} \cdot \varsigma^\rho \cdot d_{j,i}^\rho \mathbf{c}_\rho[n] * h_{j,i}^{\rho,1}[n] + \textit{interference}. \tag{28}$$

The subscript i in (27) and (28) refers to the i-th downlink slot. As the same for the preamble detection, the code sequence is used to match the received signal $r_j^i[n]$. This can also be expressed as

$$\mathbf{R}_\rho^i = \mathbf{A}_\rho \cdot \mathbf{r}^i = \left[R_\rho^i[0] R_\rho^i[1] \cdots R_\rho^i[L-1]\right] \tag{29}$$

for $\rho = 1, 2, \ldots 183$, where

$$\mathbf{A}_\rho \triangleq \frac{1}{N}\begin{bmatrix} c_\rho^*[0] & c_\rho^*[1] & \cdots & c_\rho^*[N-1] \\ c_\rho^*[N-1] & c_\rho^*[0] & \cdots & c_\rho^*[N-2] \\ \vdots & \vdots & \ddots & \vdots \\ c_\rho^*[N-L+1] & c_\rho^*[N-L+2] & \cdots & c_\rho^*[N-L] \end{bmatrix}. \tag{30}$$

The path selection is then executed that selects N_p paths from $\mathbf{R}_\rho^i$. This thus gives:

$$\begin{aligned} \hat{\mathbf{R}}_\rho^i &= f(\mathbf{R}_\rho^i) = \left[R_\rho^i[\tau_1] R_\rho^i[\tau_2] \cdots R_\rho^i[\tau_{N_p}]\right], \\ \tau_k &\in \{0, 1, \ldots, L-1\}, \end{aligned} \tag{31}$$

where τ_k is the delay of selected path index, $f(\cdot)$ represents the path selection process.

The detected sequence is the one with the maximum power. The cell ID is identified accordingly. That is,

$$\hat{\rho} = \arg\max_\rho \left\{ \sum_{i \geq 3} \sum_{p=1}^{N_p} \left|R_\rho^i[\tau_p]\right|^2 \right\}, \tag{32}$$

where $\hat{\rho}$ is the detected cell ID.

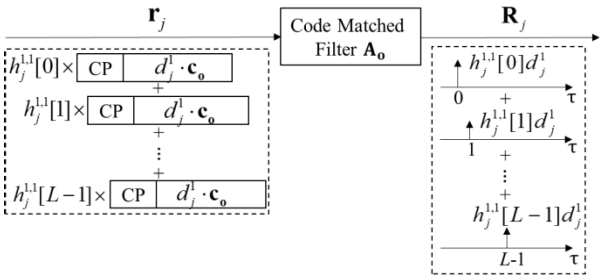

FIGURE 11. Code matched filter for code-based cell search.

V. SIMULATION

A. SIMULATION SETUP

For computer simulations, we consider the MDMA system with the cellular structure and the transceiver architecture as illustrated in [24]. The system operates in the 30 GHz mmWave band with 300 BS antennas. In addition, channel bandwidth of 200 MHz is utilized in our system that leads to the bit time of 5 ns. The radius of the cellular system is 50 m due to severe propagation loss in the mmWave band. Further, the maximum delay spread is set as 400 ns from the measurement results given by Sun and Rappaport [32]. Thus, the CP should be at least 400/5 = 80 taps to combat channel delays. Besides, the FFT size adopted is 2048 and the original un-truncated ZC sequence length is 2053. The CP length used here is 160 taps and the duration of a slot is thus 2208 taps. Moreover, the cellular system is interference limited, i.e., the background noise is neglected. Since the system is interference-limited, the exact value and unit of the transmit power are not critical. Thus the user power in one slot is set to be 1 unit. Likewise, the PCT power and SCT power in one slot are 0.5 unit and 1.5 units, respectively. The basic simulation parameters are summarized in Table 3.

We adopt a mmWave S-V channel model according to the spatial parameters given in [33]. The S-V model is a widely-used cluster-based channel model which considers path index, path amplitude, phase shift, and arrival time for both clusters and rays therein. The detail description of the model can be referred in [34].

TABLE 3. Simulation parameters.

Parameter	Value
Carrier frequency, f_c	30 GHz
Total transmission bandwidth, B_W	200 MHz
Bit time, T_c	5 ns
Maximum delay spread, τ_{max}	400 ns
Number of antennas at BS, M	300
Radius of cellular, R	50 m
Number of users in one cell, J	10,20,…,100
The maximum velocity of MS, v_{max}	108 km/hr
Length of slot, N_{slot}	2208 tap
FTT size, N	2048 tap
Length of ZC sequence, N_{zc}	2053 tap
User energy in one slot, E_u	1 unit
PCT energy in one slot, E_{PCT}	0.5 unit

Recall that the channel duration is 80 taps for the maximum delay spread of 400ns. As long as the cyclic shift is larger than 80 taps for the ZC sequence, the resulted shifted sequence has the helpful ACF and CCF properties, (16) to (17), that can be used to distinguish each other within the maximum channel delay spread. Thus, we choose 8 root indices and 23 cyclic shifts. Each shift interval is 89 samples such that $23 \times 89 < 2048$. There are totally $8 \times 23 = 184$ sequences, where the first sequence, say $\mathbf{c}_0$, is selected for the preamble. The remaining $\mathbf{c}_1, \mathbf{c}_2, \ldots, \mathbf{c}_{183}$ are used as code sequences for 183 cochannel cells. Indeed, there are many possible combinations of root indices and shift interval provided that the total number of generated sequences is enough and each shift interval is greater than the maximum channel delay spread.

B. SIMULATION RESULT

Fig. 12 shows the FCFO result. The vertical axis denotes the mean square error (MSE) of the FCFO defined as

$$
\begin{aligned}
r_j[n] &= \sum_{\rho} (\beta^{\rho})^{1/2} \cdot \varsigma^{\rho} \sum_{m} s_j^{\rho,m}[n] * h_j^{\rho,m}[n] + w_j[n] \\
&= \underbrace{\sum_{\rho} (\beta^{\rho})^{1/2} \cdot \varsigma^{\rho} \cdot \frac{1}{N} \sum_{k=0}^{N-1} \left(\sqrt{\frac{N}{2}} \delta[k - \frac{N}{2}] \right) e^{j2\pi kn/N} * h_j^{\rho,m}[n]}_{\text{w.r.t. PCT}} \\
&\quad + \underbrace{\sum_{\rho} (\beta^{\rho})^{1/2} \cdot \varsigma^{\rho} \cdot \sqrt{\frac{3}{2}} d_j^{\rho} \mathbf{c}_0[n] * h_j^{\rho,m}[n]}_{\text{w.r.t. Preamble}} \\
&\quad + \underbrace{\sum_{\rho} \sum_{m} (\beta^{\rho})^{1/2} \cdot \varsigma^{\rho} \cdot \sum_{j=1}^{J} \Theta_j^{\rho,m}[n] * h_j^{\rho,m}[n]}_{\text{w.r.t. User data}} + w_j[n]. \qquad (19)
\end{aligned}
$$

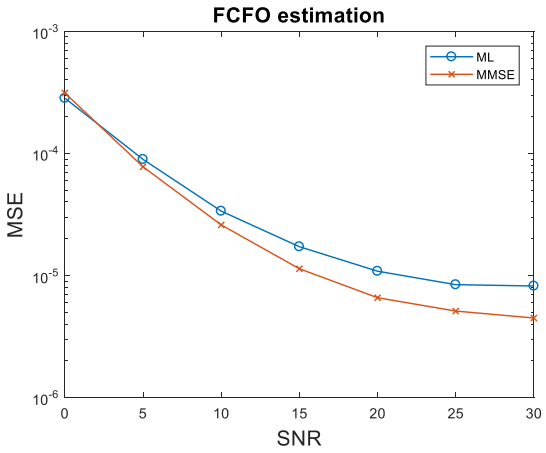

FIGURE 12. MSE of FCFO estimation for different SNRs (dB) in the multi-cell environment.

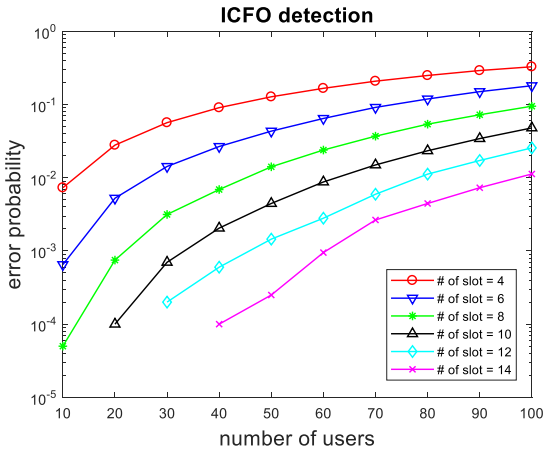

FIGURE 13. Error probability of ICFO detection in the multi-cell environment.

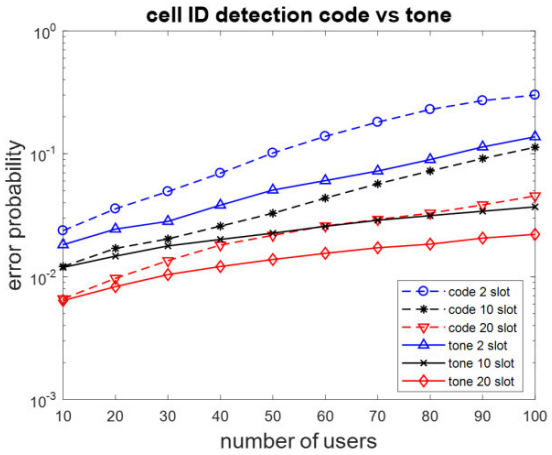

FIGURE 14. Error rate of cell ID detection in the multi-cell environment.

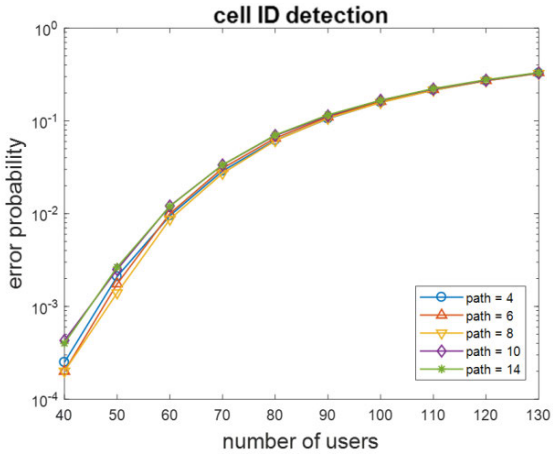

FIGURE 15. Cell ID detection performance under tone-based cell search in the single-cell environment.

$\mathrm{E}\left\{\left|\hat{\varepsilon}-\varepsilon\right|^2\right\}$. It is clear that the MMSE based detection is better than the traditional ML approach for both code and tone-based cell search schemes. The same results are obtained for both schemes since FCFO detection is based on CP structure only, which is irrelevant to cell search schemes.

Fig. 13 shows the error probability of ICFO estimation with respect to the number of users simultaneously served by the BS. The error probability of ICFO detection is the probability that the PCT is incorrectly detected. The number of slots for each curve means using different numbers of slots to conduct the combining when detecting the PCT. Results show that the ICFO detection is effective and the accuracy can be better than 10^{-2} when the number of slots is 14. In addition, results reveal that when increasing the number of slots for combining, the error probability can be decreased as expected.

The next simulation results for both methods are evaluated in terms of cell search error probability. That is, the error rates of the cell ID are plotted and investigated.

Fig.14 shows the error rate of cell ID detection. Here we accumulate over multiple slots to enhance the detection performance. 10^4 trials are executed for the simulation and an independent channel is generated for each trial. The dashed lines and solid lines refer respectively to code-based and tone-based cell search. It is clear that the tone-based cell search always outperforms the other under the same number of slots. Recall that a transmission unit contains two uplink and two downlink slots. Hence, the slot $= 2$ in the figure legend corresponds to one transmission unit for DL, slot $= 4$ corresponds to two DL units, and so on. The tone-based method performs better than the code-based method even with small number of slots. As expected, the more slots used in the accumulation, the less error probability obtained for the detection. On the other hand, as the number of user increases, the error probability also increases for all scenarios.

The previous simulation considers channels with random number of paths (channel taps). That is, we obtained the averaged performance results over all possible number of paths. However, one can also observe the effects with a fixed path number. By fixed path number we first set a positive integer Lp and generate a mmWave S-V channel. Then we select first Lp largest taps and normalize the profile to be of unit power for later simulations. To examine two methods more closely, we present single cell scenario since other-cell interference leads to the same noise level for both methods. Fig.15 and

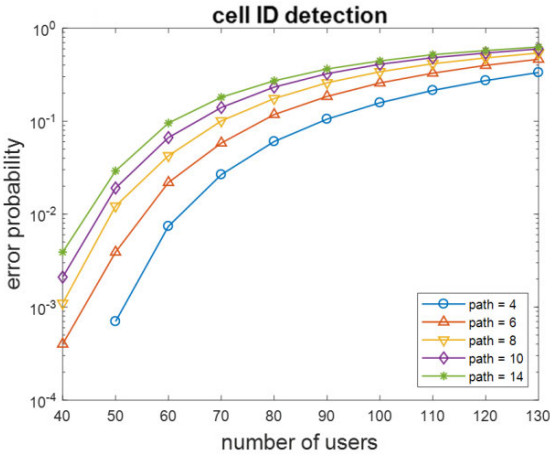

FIGURE 16. Cell ID detection performance under code-based cell search in the single-cell environment.

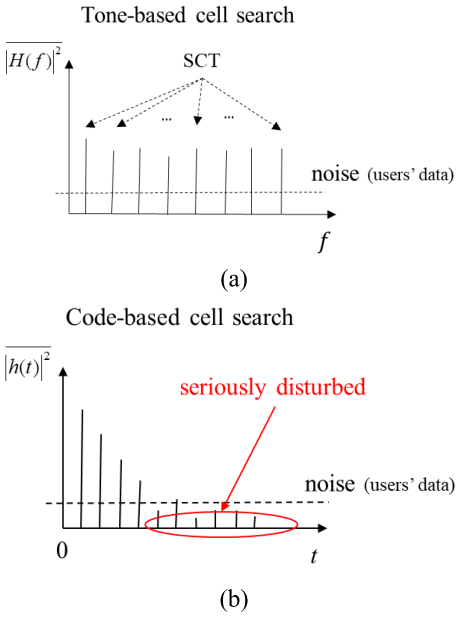

FIGURE 17. Schematic explanation for (a) Tone-based cell search and (b) Code-based cell search.

Fig.16 demonstrate the cell ID detection performance under code-based and tone-based cell search, respectively. For small path number, say $Lp = 4$, the code-based method is better than tone-based method. However, the latter method shows stable performance (with respect to path numbers) and is superior to the former for $Lp > 4$. This phenomenon is explained as follows.

Due to accumulation over multiple slots, the channel of each SCT subcarrier suffers nearly the same noise level. That is, each SCT subcarrier has nearly the same channel power to noise ratio, which is invariant to the path number. However, time-domain paths would have different channel power to noise ratios for different path powers. For channels with more paths, it is easier for each tap to be hidden below the noise level since the channel power gets more dispersed. For schematic explanation, it is shown in Fig.17 for both cases. Therefore, the tone-based cell search is better than the other for more channel taps. Since the typical 3G, 4G and 5G mobile networks all use different codes to identify different BSs, they can be seen as a kind of code-based approach. Thus, it is representative to compare the tone-based with code-based cell search methods.

VI. CONCLUSION

We investigated and compared the performance of the tone-based and the code-based cell search methods. Tone-based cell search showed superior performance over the other for general channel realizations. The main reason is that SCT subcarriers experience nearly the same channel power to noise ratio, which is invariant to the number of channel taps. It is possible that the code-based method performs better only when the tap number is always small. Simulations showed the consistent results in terms of cell search error probability. It is thus suggested to use the tone-based cell search method for general-purposed mobile communications.

APPENDIX

$$
\begin{aligned}
\left|R_{\widehat{\mathbf{c}}_q,\widehat{\mathbf{c}}_{\tilde{q}}}[\tau]\right| &\equiv \left|\widehat{\mathbf{c}}_q^H \widehat{\mathbf{c}}_{\tilde{q}}^{(\tau)}\right| \\
&= \left|\mathbf{c}_q^H(1:N)\begin{bmatrix}\mathbf{c}_{\tilde{q}}(N-\tau+1:N)\\ \mathbf{c}_{\tilde{q}}(1:N-\tau)\end{bmatrix}\right| \\
&= \Big|\mathbf{c}_q^H(1:\tau)\mathbf{c}_{\tilde{q}}(N-\tau+1:N) \\
&\quad + \mathbf{c}_q^H(\tau+1:N)\mathbf{c}_{\tilde{q}}(1:N-\tau)\Big| \\
&\le \left|\mathbf{c}_q^H(1:\tau)\mathbf{c}_{\tilde{q}}(N-\tau+1:N)\right| \\
&\quad + \left|\mathbf{c}_q^H(\tau+1:N)\mathbf{c}_{\tilde{q}}(1:N-\tau)\right| \\
&= \left|\mathbf{c}_q^H(1:\tau)\mathbf{c}_{\tilde{q}}(N-\tau+1:N)\right| \\
&\quad + \left|\begin{matrix}R_{\mathbf{c}_q,\mathbf{c}_{\tilde{q}}}[\tau]-[\mathbf{c}_q^H(N+1:N_{ZC})\mathbf{c}_q^H(1:\tau)]\\ \cdot\mathbf{c}_{\tilde{q}}(N-\tau+1:N_{ZC})\end{matrix}\right| \\
&\le |\tau| + \left\{\sqrt{N_{ZC}} + \left|\begin{matrix}[\mathbf{c}_q^H(N+1:N_{ZC})\mathbf{c}_q^H(1:\tau)]\\ \cdot\mathbf{c}_{\tilde{q}}(N-\tau+1:N_{ZC})\end{matrix}\right|\right\} \\
&\le |\tau| + \left\{\sqrt{N_{ZC}} + N_{ZC} - N + |\tau|\right\} \\
&= \sqrt{N_{ZC}} + N_{ZC} - N + 2|\tau| \qquad (33)
\end{aligned}
$$

REFERENCES

[1] G. Lui and H. Tan, "On joint symbol and frame synchronization for direct-detection optical communication systems," *IEEE Trans. Commun.*, vol. COM-35, no. 2, pp. 250–255, Feb. 1987.

[2] M. Li and W. Zhang, "A novel method of carrier frequency offset estimation for OFDM systems," *IEEE Trans. Consum. Electron.*, vol. 49, no. 4, pp. 965–972, Nov. 2003.

[3] T. S. Rappaport, *Wireless Communications: Principles and Practice*, 2nd ed. Upper Saddle River, NJ, USA: Prentice-Hall, 2002.

[4] A. Mehrotra, *GSM System Engineering*. Boston, MA, USA: Artech House, 1997.

[5] H. Holma and A. Toskala, *WCDMA for UMTS: HSPA Evolution and LTE*, 5th ed. Hoboken, NJ, USA: Wiley, 2010.

[6] *Universal Mobile Telecommunications System (UMTS); Spreading and Modulation (FDD)*, 3GPP, Standard TS 25.213, 2000.

[7] S. K. Bahl, "Cell searching in WCDMA," *IEEE Potentials*, vol. 22, no. 2, pp. 16–19, Apr. 2003.

[8] Y. P. E. Wang and T. Ottosson, "Cell search in W-CDMA," *IEEE J. Sel. Areas Commun.*, vol. 18, no. 8, pp. 1470–1482, Aug. 2000.
[9] *Physical Channels and Modulation*, 3GPP, Standard TS 36.211, 2015.
[10] S. Sesia, I. Toufik, and M. Baker, *LTE The UMTS Long Term Evolution, From Theory to Practice*. Hoboken, NJ, USA: Wiley, 2011.
[11] E. Dahkman, S. Parkvall, and J. Skold, *4G LTE/LTE-Advanced for Mobile Broadband*, 2nd ed. Cambridge, MA, USA: Academic, 2013.
[12] *1MA150: Cell Search and Cell Selection in UMTS LTE, Rohde & Schwarz Application Note*, Rohde & Schwarz, Munich, Germany, 2009, pp. 1–40.
[13] P.-Y. Tsai and H.-W. Chang, "A new cell search scheme in 3GPP long term evolution downlink, OFDMA systems," in *Proc. Int. Conf. Wireless Commun. Signal Process.*, Nanjing, China, Nov. 2009, pp. 1–5.
[14] K. Manolakis, D. M. G. Estevez, V. Jungnickel, W. Xu, and C. Drewes, "A closed concept for synchronization and cell search in 3GPP LTE systems," in *Proc. IEEE Wireless Commun. Netw. Conf.*, Apr. 2009, pp. 1–6.
[15] *NR; Physical Channels and Modulation*, 3GPP, Standard TS 38.211, 2022.
[16] *NR; Physical Layer Procedures for Control*, 3GPP, Standard TS 38.213, 2022.
[17] *Study on New Radio (NR) Access Technology*, 3GPP, Standard TR 38.912, 2022.
[18] D. Wang, Z. Mei, H. Zhang, and H. Li, "A novel PSS timing synchronization algorithm for cell search in 5G NR system," *IEEE Access*, vol. 9, pp. 5870–5880, 2021.
[19] M. Wang, D. Hu, L. He, and J. Wu, "Deep-learning-based initial access method for millimeter-wave MIMO systems," *IEEE Wireless Commun. Lett.*, vol. 11, no. 5, pp. 1067–1071, May 2022.
[20] D. Inoue, K. Ota, M. Sawahashi, and S. Nagata, "Physical cell ID detection using joint estimation of frequency offset and SSS sequence for NR initial access," *IEICE Trans. Commun.*, vol. 104, no. 9, pp. 1120–1128, Sep. 2021.
[21] J.-L. Yin, M.-C. Lee, W.-H. Hsiao, and C.-C. Huang, "A novel network resolved and mobile assisted cell search method for 5G cellular communication systems," *IEEE Access*, vol. 10, pp. 75331–75342, 2022.
[22] S. Won and S. W. Choi, "A tutorial on 3GPP initial cell search: Exploring a potential for intelligence based cell search," *IEEE Access*, vol. 9, pp. 100223–100263, 2021.
[23] J. G. Andrews, "What will 5G be?" *IEEE J. Sel. Areas Commun.*, vol. 32, no. 6, pp. 1065–1082, Jun. 2014.
[24] W. H. Hsiao and C. C. Huang, "A novel 5G TDD cellular system proposal based on multipath division multiple access," *ICACT Trans. Adv. Commun. Technol.*, vol. 5, no. 6, pp. 936–942, Nov. 2016.
[25] S. Y. Wang, W. H. Hsiao, K. L. Chiu, and C. C. Huang, "Multipath division multiple access for 5G millimeter wave cellular systems," in *Proc. IEEE GLOBECOM*, Taipei, Taiwan, Dec. 2020, pp. 1–6.
[26] W.-H. Hsiao, Y.-W. Shih, and C.-C. Huang, "Case study and performance evaluation of MDMA—A non-orthogonal multiple access scheme for 5G cellular systems," *Mobile Netw. Appl.*, vol. 23, no. 4, pp. 1035–1048, Aug. 2018.
[27] K.-L. Chiu, P.-H. Shen, B.-R. Lin, W.-H. Hsiao, S.-J.-J. Jou, and C.-C. Huang, "Design of downlink synchronization for millimeter wave cellular system based on multipath division multiple access," *IEEE Trans. Circuits Syst. I, Reg. Papers*, vol. 67, no. 9, pp. 3211–3223, Sep. 2020.
[28] D. Lee and K. Cheun, "Coarse symbol synchronization algorithms for OFDM systems in multipath channels," *IEEE Commun. Lett.*, vol. 6, no. 10, pp. 446–448, Oct. 2002.
[29] D. C. Chu, "Poly phase codes with good periodic correlation properties," *IEEE Trans. Inf. Theory*, vol. IT-18, no. 4, pp. 531–532, Jul. 1972.
[30] T. W. Chiu and C. C. Huang, "A study on initial cell search procedure in 5G MDMA massive antenna cellular system," M.S. thesis, Dept. Electron. Inf. Eng., National Chiao Tung Univ., Hsinchu, Taiwan, 2018.
[31] M.-L. Ku and C.-C. Huang, "A complementary codes pilot-based transmitter diversity technique for OFDM systems," *IEEE Trans. Wireless Commun.*, vol. 5, no. 3, pp. 504–508, Mar. 2006.
[32] S. Sun and T. S. Rappaport, "Multi-beam antenna combining for 28 GHz cellular link improvement in urban environments," in *Proc. IEEE Global Commun. Conf. (GLOBECOM)*, Atlanta, GA, USA, Dec. 2013, pp. 3859–3864.
[33] M. R. Akdeniz, Y. Liu, S. Sun, S. Rangan, T. S. Rappaport, and E. Erkip, "Millimeter wave channel modeling and cellular capacity evaluation," *IEEE J. Sel. Areas Commun.*, vol. 32, no. 6, pp. 1164–1179, Jun. 2014.
[34] A. A. M. Saleh and R. A. Valenzuela, "A statistical model for indoor multipath propagation," *IEEE J. Sel. Areas Commun.*, vol. SAC-5, no. 2, pp. 128–137, Feb. 1987.

JIA-LE YIN received the B.S. degree from the Department of Information and Electronic Engineering, Zhejiang University (ZJU). He is currently pursuing the Ph.D. degree with the Institute of Communications Engineering, National Yang Ming Chiao Tung University (NYCU). His research interest includes cell search for next-generation mobile communication systems.

WEI-HAN HSIAO (Member, IEEE) received the B.S. degree in electrical and control engineering and the Ph.D. degree in communications engineering from the National Yang Ming Chiao Tung University (NYCU), Taiwan, in 2008 and 2018, respectively. From 2018 to 2021, he worked as a Senior Engineer with the Foxconn Advanced Communication Academy, Hon Hai (Foxconn), engaging in 5G NR Cloud RAN and O-RAN Project. Since September 2021, he has been with the Department of Electrical Engineering, Chang Gung University, Taiwan. He is currently an Assistant Professor. His research interests include next generation 5G/B5G/6G mobile communication systems, millimeter wave massive MIMO technologies, and cellular communication systems.

MING-CHUN LEE (Member, IEEE) received the B.S. and M.S. degrees in electrical and computer engineering from the National Chiao Tung University, Hsinchu, Taiwan, in 2012 and 2014, respectively, and the Ph.D. degree from the Ming Hsieh Department of Electrical Engineering, University of Southern California, in 2020. From 2014 to 2016, he was a Research Assistant with the Wireless Communications Laboratory, Research Center for Information Technology Innovation, Academia Sinica, Taiwan. He is currently an Assistant Professor with the Institute of Communications Engineering, National Yang Ming Chiao Tung University. His research interests include signal processing, and design, modeling, and analysis in wireless systems and networks. He is especially working on topics relevant to caching, computing, and communication in wireless networks and integrated sensing and communication systems in recent years. He received the USC Annenberg Fellowship, from 2016 to 2020. He was awarded an Exemplary Reviewer of the IEEE TRANSACTIONS ON COMMUNICATIONS, in 2019.

CHIA-CHI HUANG was born in Taiwan, China. He received the B.S. degree in electrical engineering from the National Taiwan University, in 1977, and the M.S. and Ph.D. degrees in electrical engineering from the University of California at Berkeley, Berkeley, CA, USA, in 1980 and 1984, respectively.

From 1984 to 1988, he was a Research Fellow and the Communication System Engineer with the Corporate Research and Development Center, General Electric Company, Schenectady, NY, USA, where he worked on mobile radio communication system design. From 1989 to 1992, he was a Research Staff Member with the IBM T. J. Watson Research Center, Yorktown Heights, NY, USA, working on indoor radio communication system design. Since 1992, he has been with the National Yang Ming Chiao Tung University, Hsinchu, Taiwan, and he was a Professor with the Department of Electrical and Computer Engineering, until his retirement, in February 2021. His research interests include mobile radio, wireless communications, and cellular systems.